RSC Advances

PAPER

View Article Online
View Journal | View Issue

Cite this: *RSC Adv.*, 2022, **12**, 18936

Selective strontium adsorption using synthesized sodium titanate in aqueous solution

Gyuhyeon Kim, [a] Dae Sung Lee, [b] Harry Eccles,[c] Su Min Kim,[d] Hyun Uk Cho*[d] and Jong Moon Park *[aefg]

Received 18th April 2022
Accepted 14th June 2022

DOI: 10.1039/d2ra02494b

rsc.li/rsc-advances

Amorphous sodium titanates were synthesized using a mid-temperature sol–gel method for evaluation as selective adsorbents of strontium in the presence of cesium or metal cations (Al^{3+}, Mg^{2+}, Ca^{2+}, and Mn^{2+}) from aqueous solution. Synthesized sodium titanate showed high adsorption capacity and selectivity for strontium. The maximum adsorption capacity of strontium by sodium titanate was 193.93 mg g^{-1} in aqueous solution containing an initial concentration of 5 mM (438.60 mg L^{-1}) strontium and 5 mM (666.67 mg L^{-1}) cesium, and this sodium titanate removed 99.9% of the strontium and 40.67% of cesium from an aqueous solution that had an initial concentration of 1.14 mM (100 mg L^{-1}) strontium and 0.75 mM (100 mg L^{-1}) cesium. Strontium adsorption by synthesized sodium titanate followed pseudo-second-order kinetics and a generalized Langmuir isotherm model, and reached an adsorption equilibrium within 1 h with high adsorption capacity at equilibrium. Adsorbed strontium onto synthesized sodium titanate showed the behavior of forming a strontium titanate structure with a titanate frame *via* surface precipitation.

1 Introduction

Radionuclide pollutants have been released in large amounts by atmospheric nuclear tests, mining and milling of uranium, reprocessing of spent nuclear fuel, and operation, decontamination and decommissioning of nuclear power facilities.[1–5] Particularly, after the Fukushima Dai-ichi nuclear power plant accident many of the radionuclides have fallen to rivers, groundwater, and oceans.[6] In water, radionuclides can take various forms such as elements, precipitates, oxides, ionic forms, and organic or inorganic complexes, so suitable methods must be developed to treat each discharged radionuclide.[7]

Among these radionuclides, strontium-90 and cesium-137 have long-term environmental influence because of their high fission yield and long half-life (^{90}Sr = 28.8 years; ^{137}Cs = 30.1 years).[8,9] Particularly, strontium species have high mobility, high water solubility, and high specific radioactivity.[10] Moreover, radioactive strontium is more weakly adsorbed to particles in seawater than is radioactive cesium, which is also an abundant material in released radionuclides, because the elemental concentration of inactive strontium is significantly higher than cesium in seawater. Strontium therefore acts more strongly as a carrier and is much better stabilized than cesium.[11] Hence, effective and specific methods to treat strontium in aquatic environment are required for nuclear safety and prevention of environmental pollution.

To remove radionuclides in a water environment, many techniques are used in the nuclear industry.[12] Adsorption is a primary technique for removing radionuclides with high economic feasibility and availability.[13] Several types of organic and inorganic adsorbents such as natural zeolites, porous carbon composites, graphene oxides, ammonium molybdophosphate composites, hydroxyapatites, and sodium titanates have been used for removing strontium from aquatic circumstances.[10,14–18] In particular, sodium titanates have distinctive physico-chemical characteristics such as a low temperature compound, chemical stability at high pH, and great ability to adsorb strontium, uranium, neptunium, and plutonium in a wide range of pH and high salt concentrations.[19–22] Several sodium titanate composites such as monosodium titanates, sodium peroxotitanates, sodium nonatitanates, and sodium iron titanates have been developed for effective adsorption of strontium in aquatic environment that includes diverse radionuclides.[22–25] However, selective adsorption of strontium onto sodium titanates in aqueous solution containing cesium or

[a]*Division of Advanced Nuclear Engineering, Pohang University of Science and Technology, Pohang 37673, Republic of Korea*

[b]*Department of Environmental Engineering, Kyungpook National University, 80 Daehak-ro, Buk-gu, Daegu 41566, Republic of Korea*

[c]*School of Computing, Engineering and Physical Sciences, University of Central Lancashire, Preston PR1 2HE, UK*

[d]*Department of Marine Environmental Engineering, Gyeongsang National University, Tongyeong 53064, Republic of Korea. E-mail: hucho@gnu.ac.kr*

[e]*School of Environmental Science and Engineering, Pohang University of Science and Technology, Pohang 37673, Republic of Korea*

[f]*Department of Chemical Engineering, Pohang University of Science and Technology, Pohang 37673, Republic of Korea*

[g]*School of Integrated Technology, Yonsei University (POSTECH-Yonsei Open Campus), Pohang 37673, Republic of Korea. E-mail: jmpark@postech.ac.kr*

metal cations has not been evaluated; this competitive adsorption behavior of strontium under multicomponent conditions should be quantified.

The objectives of this study were to evaluate the selective adsorption of strontium onto sodium titanates in aqueous solution containing cesium or metal cations, and to investigate the adsorption mechanism of strontium onto sodium titanates in the presence of cesium. For these purposes, we synthesized two amorphous sodium titanates that had higher selectivity for adsorption of strontium than of cesium by using a mid-temperature (≤100 °C) sol–gel method, then evaluated their physical and chemical characteristics. We also compared their adsorption capacity, kinetics, and isotherms for adsorption of strontium.

2 Experimental

2.1 Chemical reagents

All chemical compounds and reagents were high purity laboratory grade or ACS reagents, and were used without additional purification. All were purchased from Merck KGaA: titanium isopropoxide ($Ti[OCH(CH_3)_2]_4$, ≥97%), sodium methoxide (CH_3ONa, 25 wt% in methanol), cesium nitrate ($CsNO_3$, 99%), strontium nitrate ($Sr(NO_3)_2$, ≥99%), isopropanol (C_3H_8O, ≥99.5%), sodium nitrate ($NaNO_3$, ≥99%), calcium nitrate tetrahydrate ($Ca(NO_3)_2 \cdot 4H_2O$, 99%), magnesium nitrate hexahydrate ($Mg(NO_3)_3 \cdot 6H_2O$, 99%), aluminium nitrate nonahydrate ($Al(NO_3)_3 \cdot 9H_2O$, ≥98%), manganese nitrate tetrahydrate ($Mn(NO_3)_2 \cdot 4H_2O$, ≥97%), and Triton X-100. For safety, non-radioactive cesium and strontium nitrates were used as substitutes for radioactive isotopes. Ultrapure Milli-Q water (distilled water, DW) with a resistivity of 18.2 MΩ was used in all experiments.

2.2 Preparation of sodium titanates

Sodium titanates were synthesized using a modification of a previous method.[26] First, 12 mmol of titanium isopropoxide, 6 mmol of sodium methoxide, 0.88 mL of Triton X-100, and 0.48 mL of DW were mixed, then isopropanol was added to bring the volume to 300 mL; this step was performed in a 500 mL three-neck round-bottom flask. After the chemicals had been mixed, the flask was sealed and stirred at room temperature (RT) for 24 h, then heated at 82 °C for 90 min, then purged with nitrogen until the total volume of solution reached 50 mL. While the isopropanol was evaporated, DW was simultaneously added dropwise to the flask. After heat reduction, the solution in the flask became a slurry of sodium titanate. This aqueous slurry was centrifuged, then the supernatant was removed. The remaining product was treated in two ways. First, adsorbent ST1 was obtained by washing the remaining sodium titanates three times with DW to remove any surfactant and any remaining isopropanol. Second, adsorbent ST2 was obtained by drying the remaining sodium titanates at 100 °C overnight in an oven to remove remaining aquatic residues without DW washing. Both ST1 and ST2 were stored in an oven at 60 °C until they were used in experiments.

2.3 Characterization of sodium titanates

The chemical composition of sodium titanates was analyzed using an X-ray diffractometer (XRD: X'pert PRO MPD, Malvern PANalytical B.V., Almelo, Netherlands). Surface structure of sodium titanates was observed using a scanning electron microscope (SEM: JSM-6510, JEOL Co., Ltd, Tokyo, Japan) and an energy-dispersive X-ray spectroscopy (EDS: E_{max}, Horiba, UK). Physical adsorption capacities and surface area of gas molecules on the surface of sodium titanates were quantified using a Brunauer–Emmett–Teller (BET) surface analysis device (Nanoporosity-XQ analyzer, Mirae SI Co., Ltd, Gwangju, Korea). BET surface area and pore size distribution were quantified using the Barrett–Joyner–Halenda (BJH) equation to draw an isothermal adsorption line.[27,28] The strontium adsorption mechanism of sodium titanates was analyzed using an X-ray photoelectron spectroscope (XPS: ESCALAB 250, Thermo Fisher Scientific, Waltham, U.S.).

2.4 Cesium and strontium adsorption experiments

To determine their capacities to adsorb strontium and cesium by ST1 and ST2, 0.1 g of ST1 or 0.1 g of ST2 were added to Pyrex bottles containing 100 mL solutions of 1.14 mM (100 mg L^{-1}) strontium and 0.75 mM (100 mg L^{-1}) cesium with initial pH value 7. Each bottle was sealed then stirred in a shaking incubator (VS-8480SF, Vision Science Co., Ltd, Daegu, Korea) with mixing at 200 rpm and temperature of 25 °C. Samples were collected at 10 min, 30 min, 1 h, 3 h, 6 h, 9 h, and 24 h from each bottle, then strontium and cesium concentrations were determined according to standard methods using an inductively coupled plasma-mass spectrometer (ICP-MS: ELAN DRC-e, PerkinElmer SCIEX, Wellesley, U.S.).

In addition, the competitive adsorption ability of ST2 for cesium, strontium, and metal cations (Al^{3+}, Mg^{2+}, Ca^{2+}, and Mn^{2+}) were investigated in a batch test. 0.1 g of ST2 was added to four Pyrex bottles with experimental solution (100 mg L^{-1} concentration of Al^{3+} or Mg^{2+} or Ca^{2+} or Mn^{2+} with 100 mg L^{-1} Sr and Cs, respectively) with pH value 7 were prepared. Each bottle was sealed then stirred in a shaking incubator with mixing at 200 rpm and temperature of 25 °C. Samples were collected after 24 h from each bottles and the concentration of Sr, Cs was determined by ICP-MS as described above.

Finally, to examine whether ST2 can be used as a specific strontium adsorbent in the presence of cesium, the strontium adsorption capacity (mg g^{-1}) by ST2 was measured for 48 h using aqueous solution that had initial concentrations of $1 \leq$ Sr and Cs ≤ 5 mM (87.72 mg $L^{-1} \leq$ Sr $\leq$ 438.60 mg L^{-1}, 133.33 mg $L^{-1} \leq$ Cs $\leq$ 666.67 mg L^{-1}, respectively). Experimental method was same with the batch test as discussed above with differences of concentration and time. The above experimental conditions remained unchanged during the experiment.

2.5 Kinetics and isotherms

The adsorption equilibrium capacity q_e [mg g^{-1}] was calculated as

$$q_e = \frac{(C_0 - C_e)V}{W} \quad (1)$$

where C_0 and C_e [mg L^{-1}] denote, respectively, the initial and equilibrium concentrations of adsorbate in the solution, V [L] is the volume of solution, and W [g] is the mass of adsorbent in the solution.

The kinetics of experimental data were fitted using a pseudo-first-order equation,

$$\ln(q_e - q_t) = \ln q_e - k_1 t \quad (2)$$

a pseudo-second-order equation,

$$\frac{1}{q_t} = \frac{1}{\left(k_2 (q_e)^2\right) t} + \frac{1}{q_e} \quad (3)$$

and the Elovich equation,

$$q_e = \frac{1}{\beta} \ln(1 + \alpha\beta t) \quad (4)$$

where q_t [mg g^{-1}] represents adsorption capacity for the adsorbate at time t [min], q_e [mg g^{-1}] is the adsorption equilibrium capacity for adsorbate, k_1 [min^{-1}] and k_2 [g (mg min)$^{-1}$] are the adsorption-rate constants, α [g (mg min^2)$^{-1}$] is the initial adsorption rate, and β [g (mg min)$^{-1}$] is the initial desorption coefficient.[29–31]

To calculate strontium adsorption isotherms by ST2, the data were fitted with the Langmuir equation,

$$q_e = \frac{q_m K_L C_e}{1 + K_L C_e} \quad (5)$$

the Freundlich equation,

$$q_e = K_f C_e^{1/n} \quad (6)$$

the Dubinin–Radushkevich equation,

$$q_e = q_m e^{-\beta\varepsilon^2} \quad (7)$$

and the Temkin equation,

$$q_e = \frac{RT}{b_T} \ln(A_T C_e) = B \ln(A_T C_e) \quad (8)$$

where q_e [mg g^{-1}] is the amount of adsorbate adsorbed at equilibrium, K_L [L mg^{-1}] is the Langmuir constant, K_f [L g^{-1}] is the Freundlich equation constant, q_m [mg g^{-1}] represents a theoretical maximum adsorption capacity, and C_e [mg L^{-1}] is the adsorbate concentration at equilibrium in the solution. n is the Freundlich exponent constant, β is Dubinin–Radushkevich constant of mean energy of extraction per mole of adsorbent [mol^2 J^{-1}], $\varepsilon = RT \ln(1 + 1/C_e)$ is the Polanyi potential, b_T is the Temkin isotherm constant related to adsorbent–adsorbate interactions, A_T [L g^{-1}] is the Temkin isotherm equilibrium binding constant, $R = 8.314$ [J mol^{-1} K^{-1}] is the universal gas constant, $T = 298$ K is reaction temperature, and $B = RT/b_T$ [J mol^{-1}] is a constant related to the heat of sorption.[32–35] Originpro software (version 9.0) was used to draw figures and to fit kinetics and isotherm curves by nonlinear regression methods.

3 Results & discussion

3.1 Characteristics of sodium titanates

ST1 and ST2 were aggregated solid form of amorphous phases without any crystalline structure (Fig. 1); this result agrees with

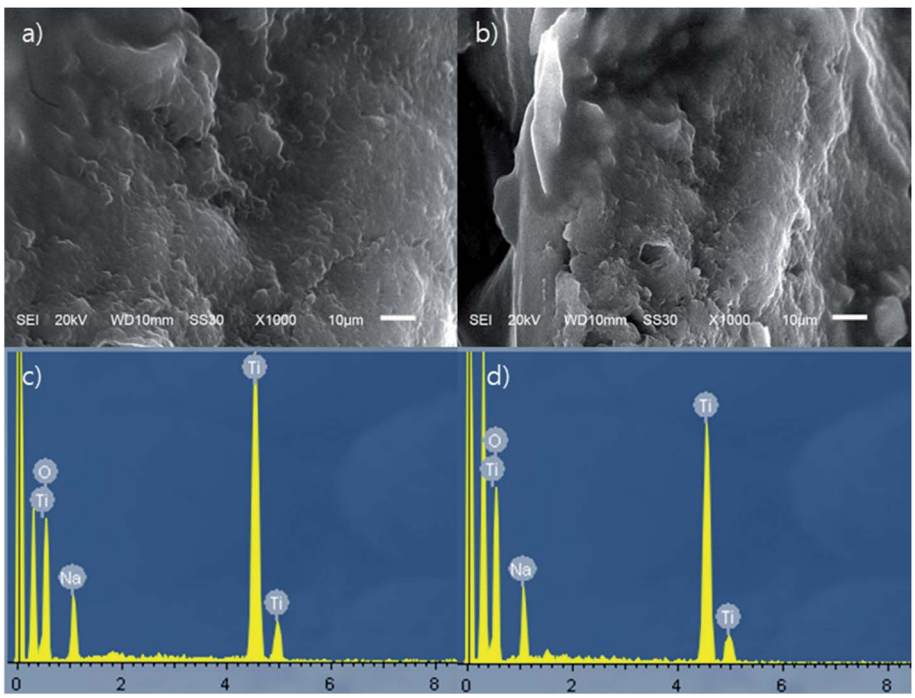

Fig. 1 SEM pictures and EDS profile data of ST1 and ST2; (a) SEM picture of ST1, (b) SEM picture of ST2, (c) EDS profile of ST1, and (d) EDS profile of ST2.

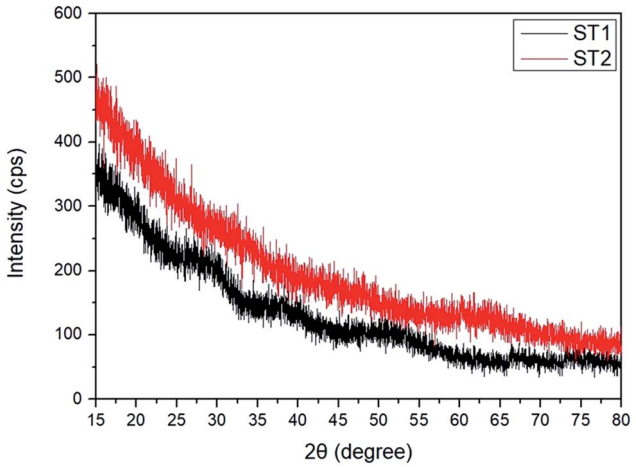

Fig. 2 XRD analysis data of ST1 and ST2.

previous reports.[36,37] The EDS spectra indicated that both ST1 and ST2 include only Na, Ti, and O. The amount of Na was smaller in ST1 than in ST2. Sodium titanates can easily hydrolysed as reaction (9), so ST1, which was synthesized using a process that involved DW washing, may have been more hydrolysed than ST2, and therefore had less Na content than ST2.[38]

$$Na_xTi_yO_z + xH_2O \rightarrow H_xTi_yO_z + xNa^+ + xOH^- \quad (9)$$

The chemical compositions of the ST1 and ST2 ($Na_{0.28}H_{1.72}TiO_3$ and $Na_{0.56}H_{1.44}TiO_3$, respectively.) in this study were estimated to be $Na_xH_{(2-x)}TiO_3$, as suggested by the ideal chemical composition of perovskite ($CaTiO_3$).[38] TiO_3 seemed to combine with one of Na or H.

XRD spectra showed no distinguishable peaks in further investigation to determine the crystal structures of ST1 and ST2 (Fig. 2); this result illustrates that both ST1 and ST2 had amorphous phase in RT condition.

To investigate the availability of Sr and Cs adsorption by ST1 and ST2, BET analysis was conducted with BJH method for determining surface area, adsorption/desorption area, and mean pore diameter of ST1 and ST2. BET surface area ($m^2\ g^{-1}$) of ST1 was 24.36 and ST2 was 244.17. BJH adsorption/desorption area ($m^2\ g^{-1}$) of ST1 was 16.54/21.78 and ST2 was 44.31/47.59. BJH mean pore diameter (nm) of ST1 was 439.1 and ST2 was 1034.4. Compared to ST1, ST2 had 10.0 times higher BET surface area, 2.1–2.6 times higher BJH adsorption/desorption area, and 2.3 times higher BJH mean pore diameter. This result may be a result of a conversion of sodium titanate to hydrogen titanate, which is described in reaction (9). DW evaporation during ST2 synthesis process also contributed to increase in surface area and pore size, and thereby facilitate the growth of sodium titanate particles when the remaining sodium titanate was supersaturated in the slurry.[39]

3.2 Cesium and strontium adsorption

Adsorption rate of Sr and Cs by ST1 and ST2 from aqueous solution containing 1.14 mM (100 mg L^{-1}) Sr and 0.75 mM (100 mg L^{-1}) Cs was examined (Fig. 3). The amounts of Sr and Cs adsorbed onto ST1 and ST2 increased as adsorption time increased to 24 h.

On ST1, the adsorption rate of Sr increased from 11.45% to 26.35% with 0.84 mM (73.65 mg L^{-1}) Sr equilibrium concentration, and the adsorption rate of Cs increased from 18.87% to 21.93% with 0.59 mM (78.07 mg L^{-1}) Cs equilibrium concentration. After 24 h, the difference was not large.

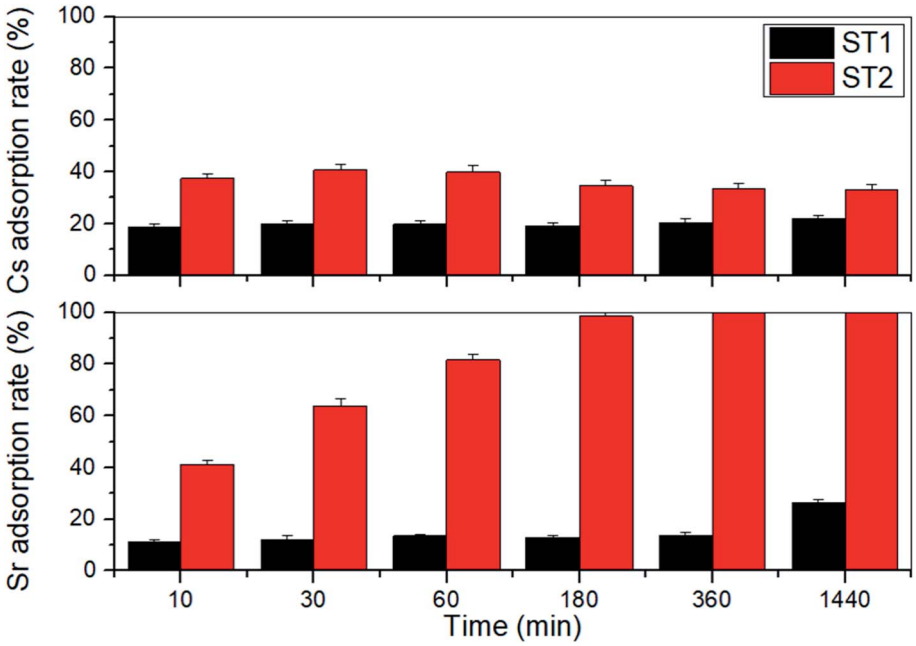

Fig. 3 Time-dependent adsorption rate of Cs and Sr by ST1 and ST2.

On ST2, the adsorption rate of Sr significantly increased from 41.24% to 99.86% with 0.16 mM (0.14 mg L^{-1}) Sr equilibrium concentration, and the adsorption rate of Cs increased from 32.91% to 40.67% with 0.44 mM (59.33 mg L^{-1}) Cs equilibrium concentration. The Sr adsorption rate was 2.5 times higher than the Cs adsorption rate (Fig. 3). A difference in adsorption rates of Sr and Cs has been reported earlier using sodium iron titanate composites.[25]

The difference of Cs, Sr adsorption rate between ST1 and ST2 can be explained that ST2 occupies larger surface area, larger mean pore diameter, and higher Na content than ST2. The ionic affinity during adsorption by sodium titanate was in the order $H^+ > Ca^{2+} > Sr^{2+} \gg Mg^{2+} > NH^{4+} > K^+ > Li^+$.[40] Therefore, ST1, which underwent DW washing that was converted $H_xTi_yO_z$ instead of $Na_xTi_yO_z$, contained more H content than ST2, resulting less adsorption rate of both Cs, Sr.

Sodium titanates have greater adsorption capacity for divalent and trivalent cations such as Sr, Np, Pu, and U than for monovalent cations such as Cs, which is normally monovalent in water.[20,37,41] However, in this trial, the amount of Sr adsorbed by sodium titanates was much higher than the amount of Cs (Fig. 3). This difference from expectation may be a result of the difference in ionic radii. Sr (125 pm) is much smaller than Cs (173 pm); this difference indicates that more Sr can be adsorbed than Cs in certain areas on sodium titanates.[42]

ST2 showed better capacity than ST1 to adsorb Sr and Cs, so ST2 was used in a test of the influence of metal cations (Al^{3+}, Mg^{2+}, Ca^{2+}, and Mn^{2+}) on Sr and Cs adsorption in a batch test (Fig. 4). Interference with Sr adsorption capacity was relatively high (10–40%) in the presence of each co-existing cation, but interference with Cs adsorption was relatively low (<10%). Ca^{2+} interfered strongly with Sr adsorption, possibly as a result of the ionic radii of the cations.[43] The ionic radii are 110 pm (Ca^{2+}), 57 pm (Al^{3+}), 86 pm (Mg^{2+}), and 81 pm (Mn^{2+}); the difference in ionic radii of Sr^{2+} (125 pm) may not be high enough to prevent interference by Ca^{2+}. However, Cs^+ (173 pm) has larger ionic radii than Sr^{2+}; this seemed to be less affected by co-existing cations.[43–47]

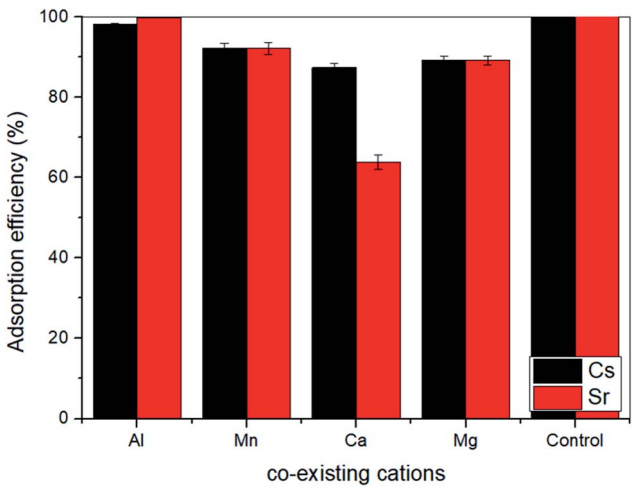

Fig. 4 Effect of co-existable cations on the adsorption of Cs and Sr by ST2 (control condition: 40.67% adsorption rate of Cs and 99.86% adsorption rate of Sr in 100 ppm Cs, Sr concentration).

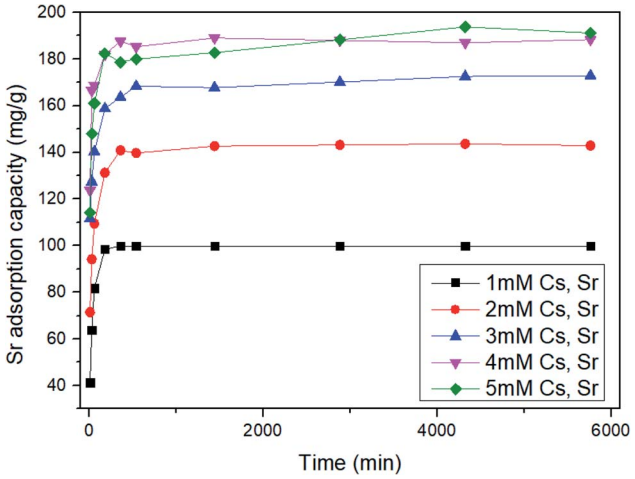

Fig. 5 Time-dependent equilibrium data for the adsorption capacity of Sr by ST2.

To examine whether ST2 can be used as a specific Sr adsorbent in the presence of Cs, the Sr adsorption capacity by ST2 was quantified using aqueous solution with initial pH value 7 that had initial concentrations of 1 ≤ Cs and Sr ≤ 5 mM (Fig. 5). All Sr adsorption capacities of ST2 increased as time increased, and reached equilibrium at 96 h. The adsorption capacities of Sr at equilibrium by ST2 increased from 99.86 to 193.76 mg g^{-1} as the initial Cs and Sr concentrations increased from 1 to 5 mM. Although Sr competed with Cs for Na from ST2 during ion-exchange process, the Sr adsorption capacity obtained from adsorption experiments was higher than that in previous other studies that used aqueous solution that contained only Sr.[10,25,43,46]

3.3 Kinetics and isotherm

To understand the mechanism of Sr adsorption by ST2 equilibrium data, pseudo-first order, pseudo-second order, and

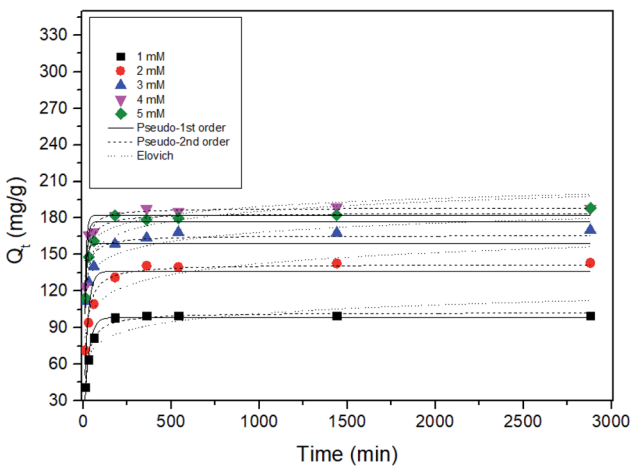

Fig. 6 Non-linear adsorption kinetics for the adsorption of Sr by ST2 at different initial Cs, Sr concentrations.

Table 1 Kinetic model parameters for the adsorption of strontium by ST2

		Pseudo-first order			Pseudo-second order			Elovich		
Initial conc. (mM)	$q_{e,exp}$ (mg g^{-1})	$q_{e,cal}$ (mg g^{-1})	k_1 (min^{-1})	r^2	$q_{e,cal}$ (mg g^{-1})	k_2 (g mg^{-1} min^{-1})	r^2	α (g (mg min^2)$^{-1}$)	β (g (mg min)$^{-1}$)	r^2
1.000	99.864	98.644	0.038	0.944	102.694	0.001	0.986	244.873	0.099	0.745
2.000	142.911	136.326	0.046	0.774	142.096	0.001	0.956	726.620	0.077	0.859
3.000	172.943	158.856	0.102	0.542	165.744	0.001	0.884	6.708×10^4	0.093	0.883
4.000	188.991	182.445	0.108	0.872	188.288	0.001	0.979	2.835×10^6	0.103	0.687
5.000	197.757	177.274	0.089	0.788	184.012	0.001	0.975	9.893×10^4	0.086	0.777

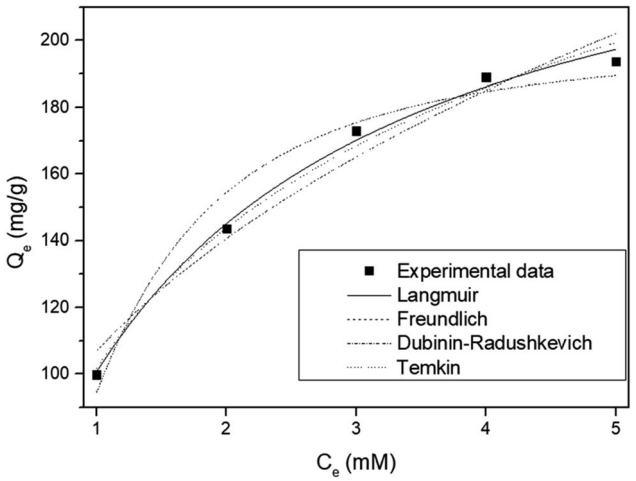

Fig. 7 Non-linear adsorption isotherm models for strontium by ST2 at different concentration at equilibrium.

Table 2 Isotherm model parameters for the adsorption of strontium by ST2

Langmuir		Freundlich		Dubinin–Radushkevich		Temkin	
K_L	0.633	K_f	106.880	q_m	199.564	A_T	5.326
q_m	259.730	n	2.526	B	1.557	b_T	37.348
r^2	0.993	r^2	0.955	r^2	0.958	r^2	0.985

Elovich kinetic models were fitted using non-linear regression analysis (Fig. 6) and kinetic parameters were obtained (Table 1). Among the kinetic models, the correlation coefficients from the pseudo-second kinetic model were the highest for $1 \leq$ Cs and Sr ≤ 5 mM; this result indicates that the pseudo-second kinetic model showed the best fit to the experimental data. This kinetic model provides information on the Sr adsorption mechanism, which entails a fast initial step that is limited by general diffusion, then a slow second step that is limited by diffusion in small pores or by slow adsorption.[25,48]

To determine the mechanism of Sr adsorption onto ST2, Langmuir, Freundlich, Dubinin–Radushkevich, and Tempkin adsorption isotherm models were applied (Fig. 7). The isotherm parameters showed that the equilibrium data were fitted best by the Langmuir isotherm (Table 2). The Langmuir isotherm suggests that Sr adsorption onto a solid surface seemed to entail a kinetic principle which is a continuous bombardment process of molecules onto the surface, with corresponding molecules' desorption or evaporation from the surface, with zero net accumulation rate at the surface.[32] ST2 is amorphous, so Sr adsorption by ST2 could follow the generalized Langmuir adsorption model, in which an amorphous material that is treated as a continuum consists of an intractable number of adsorption sites with various adsorbate affinities. Adsorbate–adsorbent interactions are negligible, so the adsorption isotherm follows the binding energy distribution of adsorption sites.[49]

The maximum Sr adsorption capacity obtained by Langmuir isotherm model was compared with other synthetic adsorbents that were reported for candidates of Sr adsorption.[10,25,43,50] ST2 has the highest Sr adsorption capacity among synthetic adsorbents that include sodium titanate species under the condition

Table 3 A comparative summary of Sr adsorption capacity and solution condition between different adsorbents (maximum Sr adsorption capacity was calculated by Langmuir isotherm model)

Materials	Compositions	Maximum Sr adsorption capacity (mg g^{-1})	Solution condition	Ref.
RSBC beads	Rice straw-based biochar	175.95	Sr only	43
Barium-sulfate-impregnated reduced graphene oxide	$BaSO_4$·rGO	232.89	Sr only	10
Sodium iron titanate	NaFeTiO	233.5	Sr only	25
Sodium titanate	$Na_{0.90}H_{1.10}Ti_2O_5$	238.26	Sr only	50
Sodium titanate	$Na_{0.56}H_{1.44}TiO_3$	259.73	Cs, Sr	This work

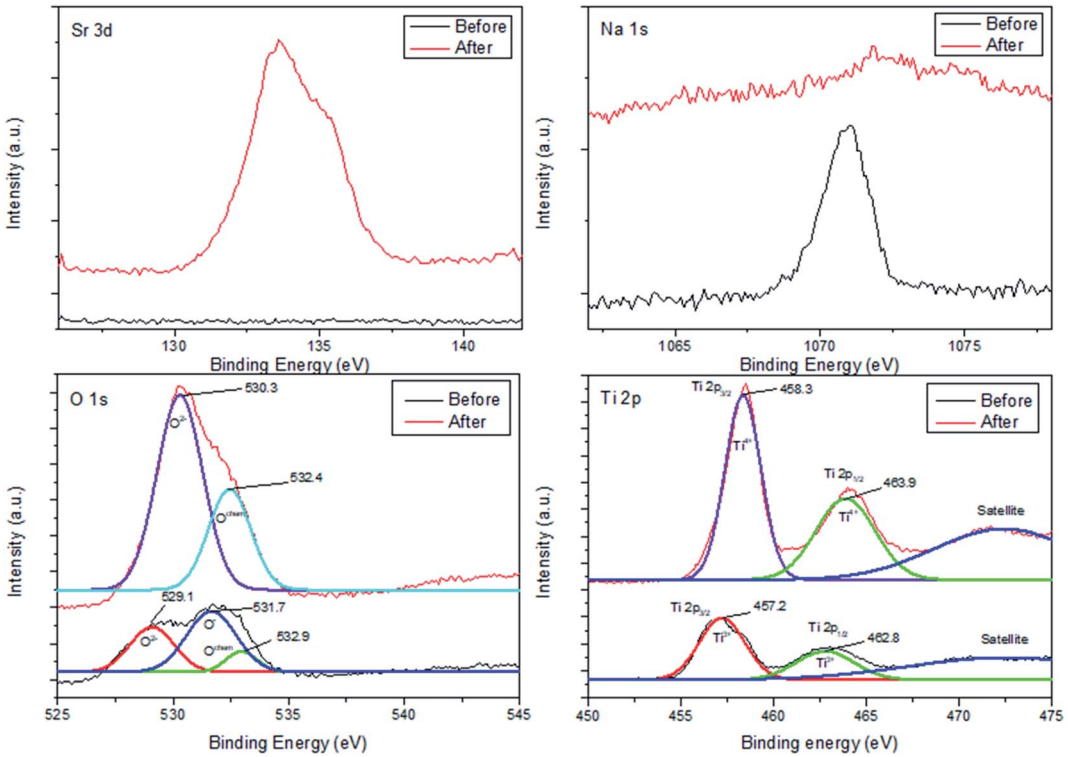

Fig. 8 XPS spectra of ST2 before and after Sr adsorption.

that Sr and Cs co-exist in aqueous solution, while other studies were conducted using aqueous solution that contains only Sr (Table 3).

3.4 Suggested mechanism of Sr adsorption on ST2

To elucidate chemical balance state and surface chemistry of Sr adsorption on ST2, XPS was conducted to identify surface

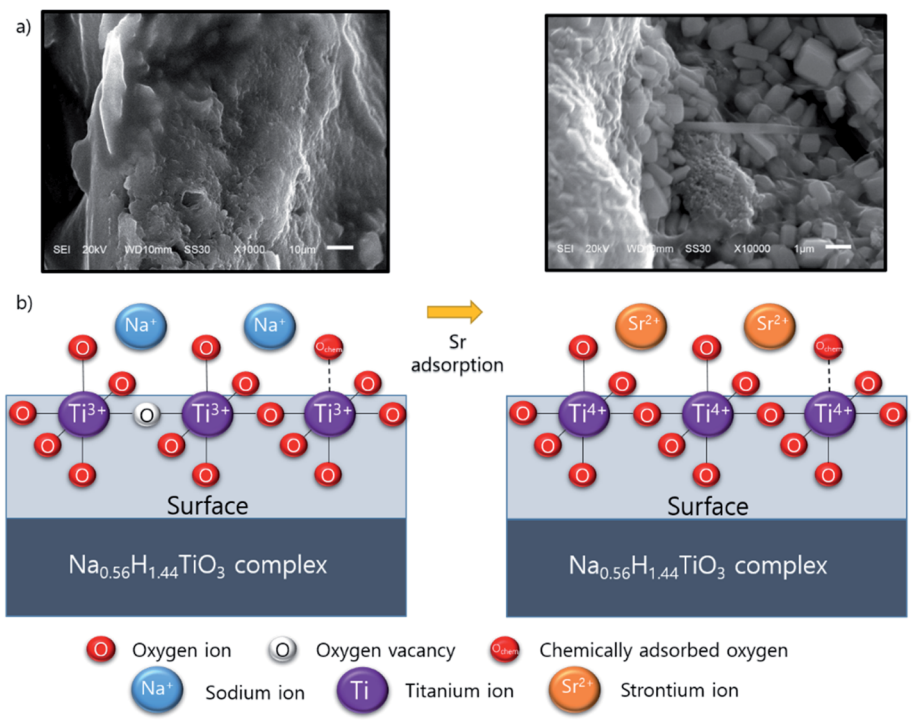

Scheme 1 Conceptual illustration of Sr adsorption mechanism onto ST2; (a) SEM picture of ST2 surface and after Sr adsorption, (b) possible mechanism of Sr adsorption onto ST2.

chemical composition and bonding configuration of ST2 before and after Sr adsorption (Fig. 8).

The XPS spectrum of Sr 3d had no distinctive peaks before Sr adsorption, but showed a distinctive peak at binding energy of 133.6 eV after Sr adsorption. This result illustrates that Sr ions had been adsorbed onto ST2.

In contrast, the XPS spectrum of Na 1s showed a distinctive peak at 1071.1 eV before Sr adsorption, but no distinctive peaks after Sr adsorption. This result indicates that Na ions had been released from ST2. This observation is consistent with a previous inference that ion exchange between Sr and Na ions occurs on the surface of ST2.[51]

In the XPS spectrum of O 1s, a binding energy peak appeared at 531.7 eV with a shoulder peak at 529.1 eV before Sr adsorption; this peak can be deconvoluted to three single peaks, which correspond to the "O^{2-}" ions (529.1 eV) in transition metal oxides and alkaline-earth oxides, "O^{-}" ions (531.7 eV) that compensate for deficiencies in the subsurface of transition metal oxides (oxygen vacancy), and O^{chem} (532.9 eV) ions that are chemically adsorbed to the surface of metal oxides.[52–54] After Sr adsorption, the XPS spectrum of O 1s showed a distinct peak at 530.2 eV, which is attributed to O^{2-} ions and a peak at 532.4 eV attributed to O^{chem}; this result implies that O^{-} ions had been converted to O^{2-} ions and that O^{2-} ions dominated on the surface of ST2.

The XPS spectrum of Ti 2p before Sr adsorption was fitted as three peaks: 457.2 eV for Ti $2p_{3/2}$ of Ti^{3+}, 462.8 eV for Ti $2p_{1/2}$ of Ti^{3+}, and some satellites. After Sr adsorption, the spectrum showed different peaks: 458.3 eV for Ti $2p_{3/2}$ of Ti^{4+}, 463.9 eV for Ti $2p_{1/2}$ of Ti^{4+}, and some satellites.[55] These results indicate that Ti ions on the surface of ST2 underwent reduction reactions during Sr adsorption.

The XPS results suggest that Sr adsorption mechanism onto ST2 as follows: Before Sr adsorption, Na ions existed in $Na_{0.56}H_{1.44}TiO_3$ complex which contains Ti^{3+} ions chemically bonded with "O^{-}" ion and O^{chem} at the surface. When Sr adsorption began, Sr ions from the aqueous solution were located in surface of ST2 instead of Na ions *via* ion-exchange process, then Sr forms the crystalline substances by surface precipitation, resulting in the presence of Ti^{4+}-based metal oxides by oxidation of Ti^{3+} on the surface of ST2 (Scheme 1). This ion-exchange model between Na and Sr was observed in other studies of Sr adsorption using titanate nanorods and mats.[50,56] SEM observations of ST2 after Sr adsorption detected cube-shaped crystals which are quite similar in shape to $SrTiO_3$ crystals as an evidence for Sr adsorption on ST2 *via* surface precipitation.[57,58]

4 Conclusions

Sodium titanate ST2 ($Na_{0.56}H_{1.44}TiO_3$) was synthesized using a modified mid-temperature sol–gel method. ST2 has amorphous structure, high capacity to adsorb Sr, and high selectivity to adsorb Sr even in the presence of Cs and metal cations (Al^{3+}, Mg^{2+}, Ca^{2+}, Mn^{2+}) in aquatic solution with initial pH value 7. Sr adsorption by ST2 in aquatic solution with initial pH value 7 followed pseudo-second-order kinetics and generalized Langmuir isotherm model. Adsorbed Sr ions onto ST2 involved formation of a strontium titanate structure ($SrTiO_3$) with titanate frame of ST2 by surface precipitation. However, a comprehensive study including pH, background electrolyte change and binary systems containing only the competing ions is required for understanding surface complexation model of Sr in ST2. Moreover, further investigations about Sr adsorption on ST2 are still needed to solve the detailed mechanism of Ti^{3+} oxidation. In summary, ST2 can be a good candidate for use to adsorb Sr from Cs-containing aqueous solutions.

Author contributions

H. E. conceived the experiments and G. K. performed the experiments. G. K., S. M. K. and H. U. C. analyzed the data. G. K. and H. U. C. wrote the manuscript. D. S. L. reviewed the manuscript. J. M. P. revised the manuscript. All authors have read and agreed to the published version of the manuscript.

Conflicts of interest

There are no conflicts to declare.

Acknowledgements

This work was supported by the National Research Foundation of Korea (NRF) grant funded by the Korea government (MSIT) (No. 2021R1G1A1095424). This research was also supported by an NRF grant from the Korean government (MSIP) (NRF-2015M2A7A1000194).

References

1 D. Yang, S. Sarina, H. Zhu, H. Liu, Z. Zheng, M. Xie, S. V. Smith and S. Komarneni, *Angew. Chem., Int. Ed.*, 2011, **50**, 10594–10598.
2 L. Nilsson and E. Forssberg, *Miner. Eng.*, 1988, **1**, 295–310.
3 O. Roth, D. Cui, C. Askeljung, A. Puranen, L. Z. Evins and K. Spahiu, *J. Nucl. Mater.*, 2019, **527**, 151789.
4 T. Y. Kong, S. Kim, Y. Lee, J. K. Son and S. J. Maeng, *Nucl. Eng. Technol.*, 2017, **49**, 1772–1777.
5 A. R. Lang, D. L. Engelberg, C. Walther, M. Weiss, H. Bosco, A. Jenkins, F. R. Livens and G. T. W. Law, *ACS Omega*, 2019, **4**, 14420–14429.
6 N. Casacuberta, P. Masqué, J. Garcia-Orellana, R. Garcia-Tenorio and K. O. Buesseler, *Biogeosciences*, 2013, **10**, 3649–3659.
7 N. R. Council, *Groundwater and Soil Cleanup: Improving Management of Persistent Contaminants*, The National Academies Press, Washington, DC, 1999.
8 P. Misaelides, in *Water Treatment Technologies for the Removal of High-Toxicity Pollutants*, ed. M. Václavíková, K. Vitale, G. P. Gallios and L. Ivaničová, Springer Netherlands, Dordrecht, 2010, pp. 183–191.
9 M. A. Olatunji, M. U. Khandaker, H. N. M. E. Mahmud and Y. M. Amin, *RSC Adv.*, 2015, **5**, 71658–71683.
10 J. Jang and D. S. Lee, *J. Nucl. Mater.*, 2018, **504**, 206–214.

11 P. P. Povinec, K. Hirose and M. Aoyama, *Environ. Sci. Technol.*, 2012, **46**, 10356–10363.
12 Waste Technology Section International Atomic Energy Agency, *Combined methods for liquid radioactive waste treatment Final report of a co-ordinated research project 1997–2001*, Vienna, 2003, vol. 1336.
13 K. C. Khulbe and T. Matsuura, *Appl. Water Sci.*, 2018, **8**, 1–30.
14 M. W. Munthali, E. Johan, H. Aono and N. Matsue, *J. Asian Ceram. Soc.*, 2015, **3**, 245–250.
15 S. Baik, H. Zhang, Y. K. Kim, D. Harbottle and J. W. Lee, *RSC Adv.*, 2017, **7**, 54546–54553.
16 Y. Park, C. Kim, W. S. Shin and S.-J. Choi, *J. Nucl. Fuel Cycle Waste Technol.*, 2013, **11**, 259–269.
17 S. S. Metwally, I. M. Ahmed and H. E. Rizk, *J. Alloys Compd.*, 2017, **709**, 438–444.
18 A. Clearfield and J. Lehto, *J. Solid State Chem.*, 1988, **73**, 98–106.
19 R. W. Lynch, R. G. Dosch, B. T. Kenna, J. K. Johnstone and E. J. Nowak, in *Symposium on the management of radioactive wastes from the nuclear fuel cycle*, International Atomic Energy Agency, Vienna, 1976, pp. 361–372.
20 M. C. Duff, D. B. Hunter, D. T. Hobbs, S. D. Fink, Z. Dai and J. P. Bradley, *J. Environ. Sci. Technol.*, 2004, **38**, 5201–5207.
21 J. Lehto and A. Clearfield, *J. Radioanal. Nucl. Chem. Lett.*, 1987, **118**, 1–13.
22 D. T. Hobbs, *J. South Carolina Acad. Sci.*, 2011, **9**, 20.
23 K. M. L. Taylor-Pashow, D. M. Missimer, A. Jurgensen and D. T. Hobbs, *Sep. Sci. Technol.*, 2011, **46**, 1087–1097.
24 M. Nyman and D. T. Hobbs, *Chem. Mater.*, 2006, **18**, 6425–6435.
25 P. Amesh, A. S. Suneesh, K. A. Venkatesan, R. Uma Maheswari and S. Vijayalakshmi, *Sep. Purif. Technol.*, 2020, **238**, 116393.
26 D. T. Hobbs, K. M. L. Taylor-Pashow and M. C. Elvington, *US Pat.*, US20140072804A1, 2014, vol. 1, p. 33.
27 S. Brunauer, P. H. Emmett and E. Teller, *J. Am. Chem. Soc.*, 1938, **60**, 309–319.
28 E. P. Barrett, L. G. Joyner and P. P. Halenda, *J. Am. Chem. Soc.*, 1951, **73**, 373–380.
29 M. P. Tavlieva, S. D. Genieva, V. G. Georgieva and L. T. Vlaev, *J. Colloid Interface Sci.*, 2013, **409**, 112–122.
30 Y. S. Ho and G. McKay, *Process Biochem.*, 1999, **34**, 451–465.
31 S. Roginsky and Y. B. Zeldovich, *Acta Phys. Chem. USSR*, 1934, **1**, 2019.
32 I. Langmuir, *J. Am. Chem. Soc.*, 1918, **40**, 1361–1403.
33 H. M. F. Freundlich, *J. Phys. Chem.*, 1906, **57**, 1100–1107.
34 A. Khandelwal, N. Narayanan, E. Varghese and S. Gupta, *Bull. Environ. Contam. Toxicol.*, 2020, **104**, 503–510.
35 M. M. Dubinin, E. D. Zaverina and L. V. Radushkevich, *Zh. Fiz. Khim.*, 1947, **21**, 151–162.
36 W. Zhang, R. Fu, L. Wang, J. Zhu, J. Feng and W. Yan, *Sci. Total Environ.*, 2019, **668**, 815–824.
37 F. F. Fondeur, D. T. Hobbs, S. D. Fink and M. J. Barnes, *Sep. Sci. Technol.*, 2005, **40**, 571–592.
38 Y. Takahatake, A. Shibata, K. Nomura and T. Sato, *Minerals*, 2017, **7**, 247–260.
39 A. Yoshida and R. Komatsu, *J. Ceram. Soc. Jpn.*, 2009, **117**, 1166–1171.
40 J. Lehto, L. Brodkin, R. Harjula and E. Tusa, in *Proceedings of the Sixth International Conference on Radioactive Waste Management and Environmental Remediation*, 1997, pp. 245–248.
41 D. T. Hobbs, M. J. Barnes, R. L. Pulmano, K. M. Marshall, T. B. Edwards, M. G. Bronikowski and S. D. Fink, *Sep. Sci. Technol.*, 2005, **40**, 3093–3111.
42 J. Luo, S. Ye, T. Li, E. Sarnello, H. Li and T. Liu, *J. Phys. Chem. C*, 2019, **123**, 14825–14833.
43 J. Jang, W. Mirana, S. D. Divine, M. Nawaz, A. Shahzad, S. H. Woo and D. S. Lee, *Sci. Total Environ.*, 2018, **615**, 698–707.
44 L. Ćurković, M. Fudurić and S. Kurajica, in *1st International Conference Corrosion and Material Protection*, 2007.
45 A. K. Vashishtha, J. Wang and W. H. Konigsberg, *J. Biol. Chem.*, 2016, **291**, 20869–20875.
46 P. Amesh, K. A. Venkatesan, A. S. Suneesh and U. Maheswari, *Sep. Purif. Technol.*, 2021, **267**, 118678.
47 J. Lehto, L. Brodkin, R. Harjula and E. Tusa, *Nucl. Technol.*, 1999, **127**, 81–87.
48 J. P. Simonin, *Chem. Eng. J.*, 2016, **300**, 254–263.
49 M. A. Al-Ghouti and D. A. Da'ana, *J. Hazard. Mater.*, 2020, **393**, 122383.
50 Y. Kondo, T. Goto and T. Sekino, *RSC Adv.*, 2021, **11**, 18676–18684.
51 R. Yi, G. Ye and J. Chen, *RSC Adv.*, 2019, **9**, 27242–27249.
52 J. C. Dupin, D. Gonbeau, P. Vinatier and A. Levasseur, *Phys. Chem. Chem. Phys.*, 2000, **2**, 1319–1324.
53 L. Q. Wu, Y. C. Li, S. Q. Li, Z. Z. Li, G. D. Tang, W. H. Qi, L. C. Xue, X. S. Ge and L. L. Ding, *AIP Adv.*, 2015, **5**, 097210.
54 F. M. Chang, S. Brahma, J. H. Huang, Z. Z. Wu and K. Y. Lo, *Sci. Rep.*, 2019, **9**, 1–9.
55 V. V. Atuchin, V. G. Kesler, N. V. Pervukhina and Z. Zhang, *J. Electron Spectrosc. Relat. Phenom.*, 2006, **152**, 18–24.
56 J. Ryu, S. Kim, H. J. Hong, J. Hong, M. Kim, T. Ryu, I. S. Park, K. S. Chung, J. S. Jang and B. G. Kim, *Chem. Eng. J.*, 2016, **304**, 503–510.
57 B. Wang, S. Shen and L. Guo, *Appl. Catal., B*, 2015, **166–167**, 320–326.
58 X. Huang, H. Liu, S. Zhang, G. Li, H. Hao, M. Cao, Z. Yao and J. Xie, *J. Mater. Sci.: Mater. Electron.*, 2018, **29**, 11546–11552.